Proceedings of the
47th IEEE Conference on Decision and Control
Cancun, Mexico, Dec. 9-11, 2008

Pull-in control during nanometric positioning by near field position sensing

S.Blanvillain*, A.Voda**, G.Besançon***
GIPSA-Lab, Department of Control Systems (Former LAG)
Grenoble, France

Abstract— **This paper deals with the pull-in control and the nanopositioning of an electrostatically actuated NEMS (Nano Electromechanical System) squeezed between two forces. It is shown that when a position sensor is driven close to a NEMS, pull-in occurs due to electrostatic forces, but also to near field forces acting at nanoscale, namely Casimir and Van der Waals forces. Pull-in conditions are investigated to find the minimum pull-in distance depending on the parameters of the system. This paper aims to demonstrate that the sensor can be driven below this minimum pull-in distance. To do so, a control strategy based on a nonlinear feedback design and on a robust pole placement/sensitivity function shaping is proposed. Furthermore, it is shown that the NEMS position can be controlled without contact while avoiding pull-in and decreasing its natural brownian motion.**

Index Terms— **NEMS, Pull-in, nano positioning, nonlinear feedback, robust control, stability.**

I. INTRODUCTION

This paper addresses the problem of the position control of a one degree of freedom NEMS actuated electrostatically and approached by a sensor. As micro systems become smaller and smaller, until nanometric dimensions [1], [2], there is a need for position sensors to follow this scale reduction [3], [4]. Thus, sensors use very weak signals, and need to be approached as close as possible to a system in order to measure its characteristics with enough accuracy. The sensor approach towards a movable mass is limited by the pull-in phenomenon [5], mainly due to electrostatic forces if the sensor is charged [6], but also due to near field forces acting at nanoscale like Van der Waals and Casimir forces, as they depend on the distance between the sensor and the mass below it [7]. Several models and techniques have been investigated in order to increase the travel range of MEMS beyond the pull-in distance. Most of the models are non-linear and often include three states: the charge of the electrostatic actuator, the position of a movable part and its velocity [8], [9]. Consequently, a panel of non-linear control methods have been worked out in order to avoid pull-in during electrostatic actuation: input-output linearization [10], passivity based design [9], flatness-based control [11], or backstepping design and control Lyapunov function [8].

The framework of the present paper is slightly different from these works. We are here in the context of approaching a charged (or not) position sensor above the movable part of a NEMS which is electrostatically actuated downwards. The aim is to approach the sensor as close as possible to the moveable part while avoiding pull-in, and to control the NEMS position. The model used does not take into account the dynamics of the sensor and actuator charges. In this way, those charges do not need to be measured or estimated, which is one of the main drawback of control strategies mentioned above: the proposed strategy only depends on the NEMS position.

The second section of the paper introduces a model of the investigated system and give description of the forces acting on it. In section III, the open-loop behavior of the system is worked out in order to study the pull-in conditions of the NEMS squeezed between two vertical forces. On this basis, the fourth section proposes a control design strategy based on exact feedback linearization [12] and pole placement technique / sensitivity function shaping [13] in order to reject disturbances generated by the sensor, and to track a given position. The corresponding results confirm it is possible to approach the sensor beyond the pull-in distance and to control the position of a NEMS while rejecting proximity forces effects such as Van der Waals or Casimir forces. In this way, manipulation of micro or nano object, without touching it and by position sensing becomes possible.

II. PRINCIPLE AND DESCRIPTION OF THE SYSTEM

A. System presentation

We propose to approach a near field sensor as close as possible to a cantilever with micro and nanometric dimensions. The extremity of the sensor is assumed to have a radius of curvature R, and is charged with a voltage V_s. The sensor is assumed to amplify displacements into voltages with a gain $C = 1,64.10^6 V/m$ and a measurement noise $n_1 = 10^{-18} V^2/Hz$. The sensor is driven step by step with a piezoelectrical actuator in the vertical direction. A schematic of the system is given in fig.1.

The origin for the referential is at the upper side of the cantilever extremity at rest, and positive displacements and forces are in the upward direction. The initial gap l_0 between the cantilever and the electrostatic actuator under it is of the order of tens of micrometers. z is the vertical deflection of

E-Mails:
* sylvain.blanvillain@gipsa-lab.inpg.fr
** alina.voda@gipsa-lab.inpg.fr
*** gildas.besancon@gipsa-lab.inpg.fr

the free end of the cantilever and z_s is the position of the sensor apex (such that $d = z_s - z$). The cantilever is squeezed between two forces: a force F_s pulling upwards generated by the sensor, and a force F_A pulling downwards controlled by a voltage V_A with an actuation noise $n_2 = 1mV/\sqrt{(Hz)}$.

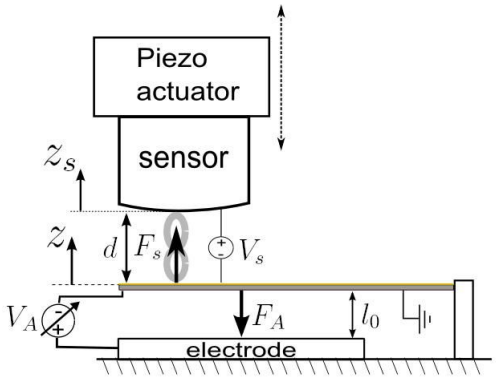

Fig. 1. Architecture of the system.

B. Finite element model of the cantilever

As in many applications, the cantilever is layered with a thin gold film in order to guarantee a good reflectivity of optical sensors and to prevent oxydation of the surface. An accurate model of such a system is obtained with a finite element method (similarly to [14]) and a modal analysis has been carried out in order to extract the ten first modes of the cantilever. This model is used for the simulation in section IV.C. A simplified model from the transfer functions of the dominant modes (the first two modes, as shown by the bold curve of fig.2) is built up from this analysis, and used in section IV for the controller design.

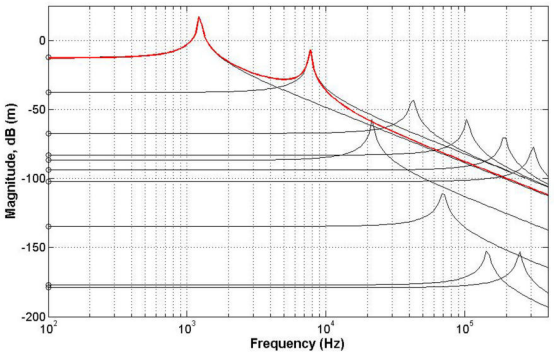

Fig. 2. Modal analysis results of a cantilever layered with a thin gold film.

C. Forces into account

1) Thermal noise: As the system is steeped by a thermal bath, its brownian motion has to be taken in account [15]. This motion is due to the random movement of particles, and can be described with the help of the equipartition theorem and Nyquist's relation [16]. The mean-square displacement $\langle z^2 \rangle$ of an oscillator resulting from thermal noise is:

$$\frac{1}{2}k_B T = \frac{1}{2}k_1 \langle z^2 \rangle \Leftrightarrow \langle z^2 \rangle = \frac{k_B T}{k_1} \quad (1)$$

This displacement is caused by a stochastic force called the Langevin force F_T exciting the cantilever, such that $\langle F_T(t) \rangle = 0$ and with a spectral density quantified by $F_T = \sqrt{4k_B T \gamma_1}$ $[N/\sqrt{(Hz)}]$ [16] (k_B is the Boltzman constant, T the temperature en Kelvin, k_1 and γ_1 the stiffness and the damping of the first mode of the cantilever, respectively).

2) Actuator Force F_A: The force pulling the cantilever bellow (fig.1) is an electrostatic force generated by the potential difference between the cantilever and the electrode. Working with small displacements, the cantilever is considered to be parallel to the electrode, and F_A can be written as [5]:

$$F_A = -\frac{A\varepsilon_0 V_A^2}{2(l_0 + z)^2} \quad (2)$$

where A is the common area of the electrode and the cantilever, ε_0 is the dielectric constant in vacuum and V_A and l_0 are respectively the voltage and the gap at rest between the cantilever and the electrode.

3) Sensor Force F_s: The force generated by the sensor on the cantilever is the sum of three forces defined below. The approaching sensor is electrically charged with a potential resulting in a voltage difference V_s between the cantilever and the sensor. Consequently, an electrostatic force generated by the sensor (half a sphere) and acting on the cantilever (plan) pull the this last one upward. This force is commonly approximated as [17]:

$$F_{elec} \approx \frac{\pi \varepsilon_0 R V_s^2}{(z_s - z)} \quad (3)$$

Where R is the radius of curvature of the sensor apex and $(z_s - z)$ the distance between the sensor and the cantilever.

The sensor is sufficiently close to the cantilever so that the Van der Waals and Casimir forces become effective. The Van der Waals force is always attractive in vacuum gap [18]. In the sphere/plan case, thanks to the Hamaker approximation, the Van der Waals force can be written as [7]:

$$F_{VdW} = \frac{HR}{6(z_s - z)^2} \quad (4)$$

Where H is the Hamaker constant ($\approx 40.10^{-20} J$).
Casimir forces takes place at longer range than Van der Waals forces, and in the case of a sphere in front of a plane, is usually approximated as in eq.(5) below, with a correction factor α given by [7] in order to take in account the finite conductivity of the materials:

$$F_{cas} \approx \alpha \frac{\hbar c \pi^3 R}{360(z_s - z)^3} \quad (5)$$

where c is the celerity of the light and $\hbar$ the reduced Planck's constant.

D. Motion equation

Gathering all forces in $F = F_T + F_A + F_{elec} + F_{VdW} + F_{cas}$, and denoting by k_i, λ_i respectively the stiffness and damping ratio of each harmonic mode, and by m the effective mass of the cantilever, the equation of the system motion approximated by its first two modes can be written as:

$$\begin{bmatrix} \dot{x}_{1p} \\ \dot{x}_{1v} \\ \dot{x}_{2p} \\ \dot{x}_{2v} \end{bmatrix} = \begin{pmatrix} 0 & 1 & 0 & 0 \\ -\frac{k_1}{m} & -\frac{\gamma_1}{m} & 0 & 0 \\ 0 & 0 & 0 & 1 \\ 0 & 0 & -\frac{k_2}{m} & -\frac{\gamma_2}{m} \end{pmatrix} \begin{bmatrix} x_{1p} \\ x_{1v} \\ x_{2p} \\ x_{2v} \end{bmatrix} + \begin{pmatrix} 0 \\ \frac{1}{m} \\ 0 \\ \frac{1}{m} \end{pmatrix} \cdot F(z, z_s, V_s, V_a) \quad (6)$$

With the output $z = (1\ 0\ 1\ 0) \cdot (x_{1p}\ x_{1v}\ x_{2p}\ x_{2v})^T$. $(x_{1p}\ x_{1v})^T$ and $(x_{2p}\ x_{2v})^T$ are position and velocity vectors of the first and second modes, respectively. It can be noticed [5] that there is a positive feedback in this system which leads to pull-in against the electrode (out of the scope of this paper), but also against the sensor. The next section is dedicated to this phenomenon, depending of the parameters of the system.

III. Pull-in analysis (open loop behavior)

This section deals with the minimal possible distance between the sensor and the mass before instability, *i.e.* pull-in. The two modes state space model (6) can be written in frequency domain as a sum of two single mode systems [19]: $G = G_1 + G_2$. The denominator of the two-modes transfer function is the product of the denominators of each single mode systems. Hence, the two modes system is stable if each single mode system is stable.
The model of the i^{th} mode is of the form:

$$\begin{bmatrix} \dot{x}_{ip} \\ \dot{x}_{iv} \end{bmatrix} = \begin{pmatrix} 0 & 1 \\ -\frac{k_i}{m} & -\frac{\gamma_i}{m} \end{pmatrix} \begin{bmatrix} x_{ip} \\ x_{iv} \end{bmatrix} + \begin{pmatrix} 0 \\ \frac{1}{m} \end{pmatrix} \cdot F(z, z_s, V_s, V_a) \quad (7)$$

with the output $z = x_{ip}$. The stability of the i^{th} mode is studied through the Lyapunov indirect method [12]. If x_0 is an equilibrium position of the mass, and under the assumptions $z > l_0$ and $z_s > z$, the state space matrix around this equilibrium is:

$$A_{x_0} = \begin{pmatrix} 0 & 1 \\ -\frac{k_i}{m} + \frac{1}{m}\frac{\partial F}{\partial x_{ip}} & -\frac{\gamma_i}{m} \end{pmatrix} \quad (8)$$

Then, x_0 is asymptotically stable if the real part of the eigenvalues of A_{x_0} are strictly negative, *i.e.*, for a two modes model ($i = 1, 2$):

$$-k_1 + \frac{\partial F}{\partial z} < 0 \quad and \quad -k_2 + \frac{\partial F}{\partial z} < 0 \quad (9)$$

On the other hand, pull-in happens if the left member of eq.(9) is positive or null. The lowest value of k_i is always for the first mode ($i = 1$), so the stability criteria is:

$$-k_1 + \frac{\partial F}{\partial z} < 0 \quad (10)$$

When voltages of the system V_s, V_A are fixed and the sensor is approached to the cantilever, there is a minimum distance under which the system becomes unstable [5]. In other words, the sensor can not approach the cantilever below the pull-in distance d_{PI}, distance from which the mass collapses against the sensor and remains stacked. The minimal tip/cantilever distance before pull-in depends on the system parameters and can be estimated by solving the following minimization problem:

$$\begin{cases} min(z_s - z) \\ With\ the\ following\ constraints: \\ 0V \leq V_A \leq 19V \\ 0V \leq V_s \leq 2V \\ -6.10^{-6}m < z_s\ and\ z \leq 200.10^{-9}m \\ \frac{\partial F}{\partial z} = k_1 \\ F = k_1 z \end{cases} \quad (11)$$

The minimum of $z_s - z$ is $34\ nm$ and corresponds to the lowest values of V_s and V_a, *i.e.* zero volt. Moreover, this problem prove that if a voltage V_a is initially applied to the electrode, the pull-in distance would be increased.
Because a voltage V_s of zero volt is almost never reached in practice, due to residual charges and experimental conditions, the following simulation is done with $V_s = 1V$, which increases the pull-in distance to $d_{PI} = 57,3nm$.

IV. Closed loop control

This section aims to prove that the position z of the cantilever can be controlled, even if the sensor is at a distance below d_{PI}. To do so, a feedback linearizing the electrostatic actuator nonlinearity is first applied, and a linear controller synthesis based on poles placement/sensitivity function shaping is then used to achieve a robust control. The control design is made with the simplified model of the cantilever, taking in account the two dominant modes, and the simulation is carried out with the complete model (20th order).

A. Control problem formulation

The control problem can be formulated as a servo control problem: the measured position z tracks a given reference while rejecting the forces F_{elec}, F_{VdW} and F_{cas} which increase when the sensor position z_s decreases. The complete block diagram associated to this servo problem is shown in fig.3, where n_1 and n_2 are additional measurement and actuator noises. The model of the electrostatic actuator is nonlinear since F_A is function of the square of V_A and of the inverse of the square of z. A tangent linearization around

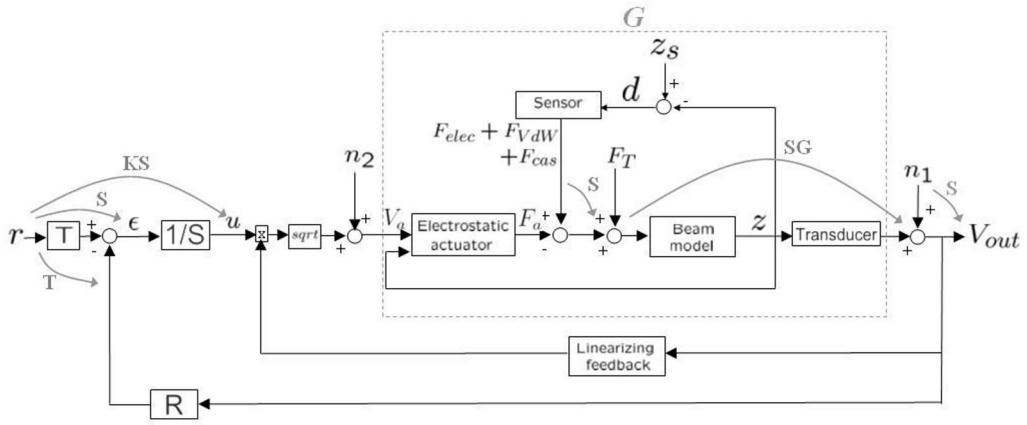

Fig. 3. Block diagram of the closed loop system.

the cantilever rest position would not be judicious, since this last one must be able to track a reference input r. In order to tackle this problem, a linearizing feedback, similarly to [10], is designed as follows:

$$V_A(t) = \sqrt{\frac{2\left(z/C + l_0\right)^2}{\varepsilon_0 A}.u(t)} \quad if\ u(t)\ \geq 0; \tag{12}$$

$$V_A(t) = 0 \quad if\ u(t)\ < 0;$$

where C is the transducer gain, $u(t)$ is the control signal generated by the RST controller, and is limited to positive values. In this manner, the non-linearity due to the electrostatic actuator is compensated, and the controller can be designed using a linear method.

B. Control specifications and design

Using the block diagram of fig.3, stability and performances requirements can now be expressed by means of constraints on the closed loop sensitivity functions [20]. These constraints will be used for the controller design and performances analysis. In the case of an RST controller and when the plant G can be explained as $G(s) = B(s)/A(s)$, sensitivity functions (grey arrows in fig.3) are classically defined by the following relationships:

$$\mathbf{S}(s) = A(s).S(s)/(A(s).S(s) + B(s).R(s)) \tag{13}$$

$$\mathbf{SG}(s) = G(s).\mathbf{S}(s); \quad \mathbf{KS}(s) = R(s)/S(s).\mathbf{S}(s) \tag{14}$$

$$\mathbf{T}(s) = B(s).T(s)/(A(s).S(s) + B(s).R(s)) \tag{15}$$

The output sensitivity function **S** characterizes the influence of an output disturbance on the closed loop system output. The complementary sensitivity function **T** is the transfer from the reference signal r to the closed loop system output V_s. **KS** is the input sensitivity function and characterizes the influence of an output disturbance on the control signal u. **SG** is the output sensitivity function with respect to an input disturbance.

1) Stability margin: In order to ensure sufficient stability margins, some limitation constraints must be imposed on the closed-loop sensitivity function [13], the usual ones being on **S** and **T**. The maximum $\|\mathbf{S}\|_\infty$ of the sensitivity function S should be less than 6dB (constraint 1 on fig.4). In the same way, the complementary sensitivity function maximum $\|\mathbf{T}\|_\infty$ should be less than 3,5dB. A constraint on the maximum of **KS** is added in order to prevent instability due to saturation effect in the electronic part: $\|\mathbf{KS}\|_\infty$ should be less than 15dB.

2) Tracking performances: The closed loop bandwidth must be higher than the nominal open loop system bandwidth, which is translated into constraints on **S** and **T**. The closed loop transfer function **T** should have a constant gain for frequency in the chosen bandwidth and **S** must have a slope of at least 20dB in this bandwidth (constraint 2 on fig.4). The closed loop bandwidth is chosen at the frequency of the first resonance of the cantilever, *i.e.* $7767 rad/sec$. On the other hand, the input disturbance rejection is ensured by a slope of 20dB or more on **SG** at small frequencies. This transfer function is also responsible of the amplification or attenuation of the brownian motion of the cantilever, as this motion is generated by an input disturbance F_T (the Langevin force). In order to fulfill the 'cold damping' conditions (i.e. to attenuate the amplitude of the brownian motion [6]), **SG** must be lower to its maximum in open-loop (150dB). A constraint is here fixed in order to attenuate by a factor 40 (32dB) or more the output, meaning that $\|\mathbf{SG}\|_\infty$ in closed-loop must be inferior to $150 - 32 = 118dB$ (constraint 3 on fig.4).

3) Stability and performance robustness: Although stability margins ensure basic robustness, other robustness constraints can be specified in order to handle worst-case technological dispersions or time varying parameters. The first point requires uncertainties characterization on the different physical parameters. As the control of the plant G depends on l_0 and A, the controller must be robust to dispersions in these parameters. A variation of at least 40% for these

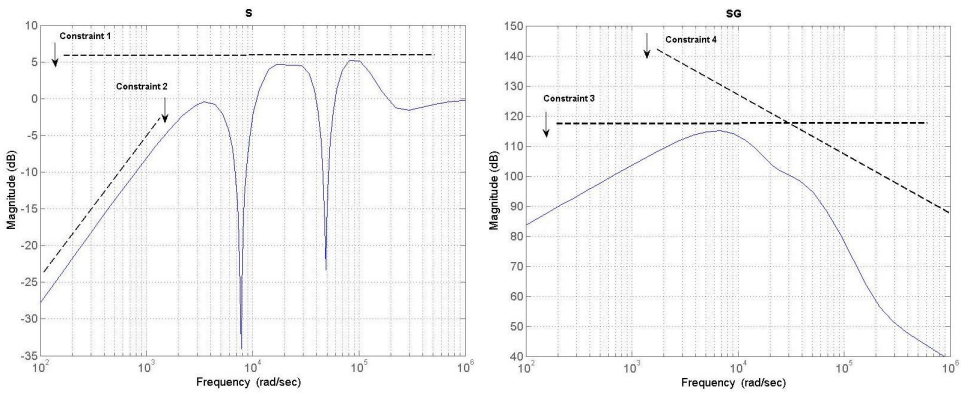

Fig. 4. Sensitivity functions **S** and **SG** of the model in closed loop.

parameters would be a fair estimation.
Robustness must also consider time varying parameters. The main parameter subject to time-variation are damping coefficients γ_i in (6) through the modification of operation conditions: temperature variations, heat dispersion during operation time... Because this coefficient can not be accurately computed, the worst case of damping coefficients dispersion is estimated to 50%. This dispersion can be modeled as a feedback uncertainty around the nominal transfer function G_i $(i = 1, 2)$ of each harmonic mode [21]:

$$\tilde{G}_i(s) = G_i(s)/(1 + \Delta W_i(s) G_i(s)) \tag{16}$$

$$W_i(s) = \frac{\delta\gamma\ s}{a_i}, \quad -1 \leq \Delta \leq 1 \tag{17}$$

where $W_i(s)$ provides the uncertainty profile (for each mode), $\delta\gamma$ is the damping coefficient variation around the nominal value and a_i is the gain of each harmonic mode transfer function times the sensor's gain C. The stability robustness condition for such an uncertainty model is:

$$\|W_i(s)\ \mathbf{GS}(s)\|_\infty \leq 1, \tag{18}$$

$$\Leftrightarrow \quad |GS(s)| \leq |1/W_i(s)|, \quad \forall f \tag{19}$$

with $W_i(s)$ so that $W_i(s) = \delta\gamma_i\ s/(a_i.10^6)$. The most restrictive constraint is obtained for $i = 2$, i.e. the uncertainty on the damping of the 2^{nd} mode. Robustness towards this time varying parameter is illustrated by the constraint 4 on fig.4.

To ensure specifications mentioned above, an RST-type controller has been designed using the pole placement technique with sensitivity function shaping described in [20]. Beyond its simplicity, this method provides an instantaneous view of the control loop performances, and furthermore, the designer sets the controller order. As the maximum order of the controller is often limited by the hardware, a maximum order of eight is imposed. The controller was designed so that the closed-loop natural frequency remains the same as the open-loop first resonance frequency (closed-loop dominant poles P_D such that $f_{CL} = 7767 rad/sec$ with $\zeta = 0,9$ as damping coefficient). The other design characteristics are the following: a filter H_S is designed as a factor of the polynomial S. It combines one integrator and a 2^{nd} order filter ($f_{H_s} = 23.10^3 rad/sec$, $\zeta = 0,4$) in order to reject the DC perturbations, to reduce the maximum of **S** under 6dB between the two resonance modes of **G**, and to fix $\|\mathbf{GS}\|_\infty$ below 118dB. Closed-loop auxiliary poles P_F are add around $2.10^5 rad/sec$ in order to lower **S** at high frequencies. This design leads to the sensitivity functions **S** and **SG** plotted in fig.4, and results in a 6th order controller.

C. Closed loop analysis and simulation results

The above controller was designed in order to comply as closely as possible with the stability and robustness constraints given in fig.4. The maxima of the sensitivity function **S** is 5,2dB. Consequently, stability margins are high enough to guaranty a good stability of the system (phase margin: $47,1 deg.$, gain margin: $6,9 dB$). The bandwidth of the closed loop system is around 7.10^3 rad/sec.
Concerning **SG**, its maximum is 115dB, which leads to an attenuation factor of 0.018 from the open-loop to the closed-loop. Constraints on **KS** are respected ($\|\mathbf{KS}\|_\infty$=2dB). Finally, stability robustness towards parametric dispersions and damping coefficient variations are very satisfactory: the designed controller is robust to more than 50% of variations of A and l_0, and to 50% of the damping ratio, as the maximum of **SG** is well below $W(s)$.

The behavior of the open loop system (plant G with the finite element model of the cantilever) is illustrated in fig.5 by the black dashed curve. The sensor is charged with 1 volt, and is driven downward step by step. Under these conditions, the cantilever collapses to the sensor due to the pull-in phenomenon when the distance between them reaches $57nm$. After pull-in, the sensor and the cantilever remain stacked. Applying the control described in the last sections leads to the other curves of fig.5. The disturbance is completely rejected with low overshoot ($11nm$ at the last piezo step). We observe that the sensor can be driven bellow the pull-in distance ($d_{PI} = 57nm$) without instability. The red dashed curve shows the robustness performance towards

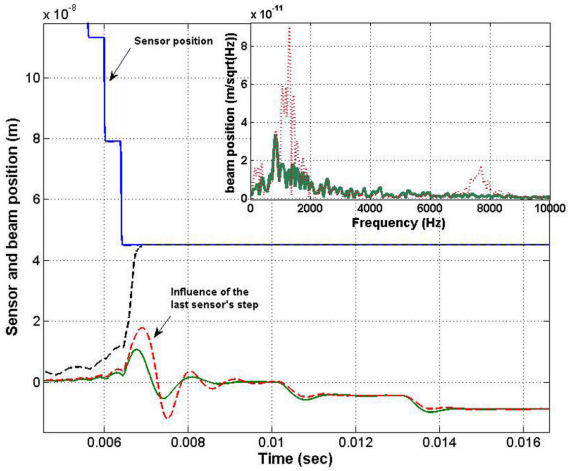

Fig. 5. Open and closed-loop behavior of the system. The top figure shows the noise spectrum at the free end of the cantilever in open loop and closed-loop.

50% variation of the coefficients used by the command, and 50% variation of the damping of the cantilever.

As predicted with the observation of the sensitivity function **SG**, the brownian motion can be significantly attenuated, even in the framework of a tracking problem. The root mean square of the brownian motion in open loop ($6.10^{-11}m/\sqrt{Hz}$) is attenuated and reaches $2,1.10^{-11}m/\sqrt{Hz}$ in closed loop. The spectrum of the noise in closed-loop and in open-loop is plotted in fig.5. According to equation (1), such an amplitude corresponds to an operating condition at a temperature of 32 $Kelvin$. As a direct consequence, it is possible to recreate the same conditions as those at a temperature much lower than the ambient one, and thus to obtain more accurate position measurements at nano-scale.
When the sensor has reached a distance of 45nm with the cantilever, two consecutive steps are applied to the cantilever reference position r. These steps show it is possible to drive the mass position with the actuator pulling it, even in the presence of near field forces.

V. Conclusion

This paper addresses the control problem of a mass squeezed between two opposite forces: a disturbance generated by a sensor and an actuator. It has first been shown that the system becomes unstable when the mass is too close to the sensor due to pull-in phenomenon. The proposed control strategy confirms it is possible to fully reject the disturbance with low overshoot and thus to avoid pull-in, to control the position of the mass and to apply the cold damping concept at the same time. As a direct consequence, it becomes possible to approach a position sensor as close as wanted to a NEMS. Moreover, attenuating the thermal noise allows to recreate conditions similar of those of very low temperature, and thus to make very accurate measurements. Moreover, this work shows that the position control of a micro or nanometric object is possible without being in contact with it: near field forces are used as a gripper to squeeze the object, and to manipulate it without contact.

References

[1] E. Ollier, L. Duraffourg, Mt. Delaye, H. Grange, S. Deneuville, J. Bernos, R. Dianoux, F. Marchi, D. Renaud, T. Baron, P. Andreucci, and P. Robert. Nems devices for accelerometers compatible with thin soi technology. *Nano/Micro Engineered and Molecular Systems, 2007. NEMS '07. 2nd IEEE International Conference on*, pages 180–185, Jan. 2007.
[2] V. Cimalla, F. Niebelschtza, K. Tonischa, Ch. Foerstera, K. Brueckner, T. Friedrichb I. Cimalla, J. Pezoldta, R. Stephana, M. Heina, and O. Ambachera. Nanoelectromechanical devices for sensing applications. *Sensors and Actuators B*, 126:24–34, 2007.
[3] M. Sumetsky, Y. Dulashko, and A. Hale. Fabrication and study of bent and coiled free silica nanowires: Self-coupling microloop optical interferometer. *Opt. Express*, 12(15):3521–3531, 2004.
[4] C.J. Lin and F.G. Tseng. A micro perot fabry sensor for nano lateral displacements sensing with enhanced sensitivity and pressure resistance. *Sensors and Actuators A*, 114:163–170, 2004.
[5] S.D. Senturia. *Microsystems Design*. Kluwer Academic, Boston, 2000.
[6] G. Jourdan, G. Torricelli, J. Chevrier, and F. Comin. Tuning the effective coupling of an afm lever to a thermal bath. *Nanotechnology*, 18(47):475502 (6pp), 2007.
[7] G. L. Klimchitskaya, U. Mohideen, and V. M. Mostepanenko. Casimir and van der waals forces between two plates or a sphere (lens) above a plate made of real metals. *Phys. Rev. A*, 61(6):062107, May 2000.
[8] G. Zhu, J. Penet, and L. Saydy. Modeling and control of electrostatically actuated mems in the presence of parasitics and parametric uncertainties. *Journal of Dynamic Systems, Measurement, and Control*, 129:786–794, November 2007.
[9] D.H.S. Maithripala, B.D. Kawade, J.M. Berg, and W.P. Dayawansa. A general modelling and control framework for electrostatically actuated mechanical systems. *Int. J. Robust Nonlinear Control*, 15:839–857, 2005.
[10] G. Besançon, A. Voda, and E. Colinet. Towards oscillation control in a vibrating cantilever nonlinear nems. In *Proceedings of the European Control Conference, Kos, Greece*, pages 2582–2586, July 2007.
[11] G. Zhu, J. Levine, L. Praly, and Y.-A. Peter. Flatness-based control of electrostatically actuated mems with application to adaptive optics: A simulation study. *Microelectromechanical Systems, Journal of*, 15(5):1165–1174, Oct 2006.
[12] A. Isidori. *Nonlinear control systems*. Springer-Verlag, 1995.
[13] I.D. Landau. *System identification and control design*. Englewood Cliffs, 1990.
[14] D.-A. Mendels, M. Lowe, A. Cuenat, M. G. Cain, E. Vallejo, D. Ellis, and F. Mendels. Dynamic properties of afm cantilevers and the calibration of their spring constants. *Journal of Micromechanics and Microengineering*, 16(8):1720–1733, 2006.
[15] S. Rast, C. Wattinger, U. Gysin, and E. Meyer. The noise of cantilevers. *Nanotechnology*, 11(3):169–172, 2000.
[16] C. Kittel. *Elementary Statistical Physics*. Mineola, New York : Dover Publications, 1958.
[17] S. Belaidi, P. Girard, and G. Leveque. Electrostatic forces acting on the tip in atomic force microscopy: Modelization and comparison with analytic expressions. *Journal of Applied Physics*, 81(3):1023–1030, 1997.
[18] H.C. Hamaker. The london - van der waals attraction between spherical particules. *Physica*, Vol.4:pp.1058–1072, 1937.
[19] M. R. Hatch. *Vibration Simulation Using MATLAB and ANSYS*. Chapman & Hall, 2000.
[20] I.D. Landau, R. Lozano, and R. M'Saad. *Adaptative control*. London, 1997.
[21] A.R. Tannenbaum J.C. Doyle, B.A. Francis. *Feedback control theory*. 1992.